QUANTUM FLUIDS

Giant vortex clusters in a two-dimensional quantum fluid

Guillaume Gauthier[1]*, Matthew T. Reeves[2]*, Xiaoquan Yu[3], Ashton S. Bradley[3], Mark A. Baker[1], Thomas A. Bell[1], Halina Rubinsztein-Dunlop[1], Matthew J. Davis[2], Tyler W. Neely[1]†

Adding energy to a system through transient stirring usually leads to more disorder. In contrast, point-like vortices in a bounded two-dimensional fluid are predicted to reorder above a certain energy, forming persistent vortex clusters. In this study, we experimentally realize these vortex clusters in a planar superfluid: a ^{87}Rb Bose-Einstein condensate confined to an elliptical geometry. We demonstrate that the clusters persist for long time periods, maintaining the superfluid system in a high-energy state far from global equilibrium. Our experiments explore a regime of vortex matter at negative absolute temperatures and have relevance for the dynamics of topological defects, two-dimensional turbulence, and systems such as helium films, nonlinear optical materials, fermion superfluids, and quark-gluon plasmas.

An isolated system that is initially stirred will in most cases eventually achieve quiescent thermodynamic equilibrium. However, in some systems, the near decoupling of particular degrees of freedom can result in an isolated subsystem with a different time scale for equilibration (*1*). The subsystem can exhibit highly correlated and nonuniform thermal equilibria (*2*–*4*). As recognized by Lars Onsager (*4*), a prototypical example is a system of N point vortices (*5*) contained within a bounded two-dimensional (2D) fluid. This model predicts that, given sufficient decoupling between 2D and 3D flow and negligible viscous dissipation, high-energy fluid flow yields low-entropy equilibria that exhibit large-scale aggregations of like-circulation vortices (*4*). This is markedly different than the behavior of vortices in 3D fluids (*6*, *7*). Onsager's theory has provided some understanding of diverse classical quasi-2D systems such as turbulent soap films (*8*), guiding-center plasmas (*9*), self-gravitating systems (*10*), and Jupiter's Great Red Spot (*11*). However, quantitative demonstration of point-vortex statistical mechanics is challenging; although the dynamics in 2D classical fluids can lead to vortex cluster growth, these vortices are continuous and cannot be realistically modeled by discrete points (*12*, *13*). Onsager was aware of this limitation and noted the model would be more realistic for 2D superfluids, where vortices are discrete, with circulations constrained to $\Gamma = \pm h/m$, where h is Planck's constant and m is the mass of a superfluid particle. The physical realization of high-energy point-vortex clusters in any fluid system has, however, remained elusive.

The incompressible kinetic energy of an isolated 2D fluid containing N point vortices can be expressed in terms of the relative vortex positions (*5*). In an unbounded uniform fluid, it has the form

$$H = -\frac{\rho_0}{4\pi}\sum_{i\neq j}\Gamma_i\Gamma_j \ln\left|\frac{\mathbf{r}_i - \mathbf{r}_j}{\xi}\right| \qquad (1)$$

where ρ_0 is the 2D fluid density, ξ is a short-range cutoff scale, and Γ_i is the circulation of a vortex at position $\mathbf{r}_i$; the sign of Γ_i indicates the direction of rotation. Onsager's key insight was that, because Eq. 1 is determined by the positions $\mathbf{r}_i$, the available phase space for a confined fluid becomes bounded by the area of the container (*4*). This property dramatically alters the system's thermodynamic behavior.

The equilibrium phases of a neutral N-vortex system in a bounded elliptical region are shown schematically in Fig. 1, A to D. Thermodynamic equilibria maximize the entropy (Fig. 1E), given by $S(E) = k_B \ln W(E)$, where the density of states $W(E) = \xi^{-2N}\int\prod_i^N d^2\mathbf{r}_i\,\delta\left(E - H(\{\mathbf{r}_i\})\right)$ measures the number of possible vortex configurations at a given energy E (*14*); k_B is Boltzmann's constant. The vortex temperature (Fig. 1F) is given by $T = (\partial S/\partial E)^{-1}$. The low-energy, positive-temperature phase ($T > 0$) consists of bound vortex-antivortex pairs (Fig. 1A). As the energy increases, these pairs unbind (*15*), increasing the average nearest-neighbor distance ℓ (Fig. 1E), until the vortex distribution becomes completely disordered (Fig. 1B), marking the point of maximum entropy ($T = \infty$). However, owing to the bounded phase space, this point occurs at finite energy E_m; at still higher energies, vortices reorder into same-sign clusters (*2*, *4*), thus decreasing the entropy and yielding negative absolute temperatures ($T < 0$). At a sufficiently high energy, the system undergoes a clustering transition ($T = T_c$) (*16*); here, the vortices begin to polarize into two giant clusters of same-circulation vortices (Fig. 1C), whose structures are determined by the shape of the container. The major-axis projection of the dipole moment, $D = N^{-1}\left|\sum_j \mathrm{sgn}(\Gamma_j)x_j\right|$, serves as an order parameter for the clustering transition (*14*); below the transition $D = 0$, whereas above the transition it begins to grow as $D \propto (E - E_c)^{1/2}$ (Fig. 1F) (*16*). Finally, in the so-called supercondensation limit $\xi \to 0$, $E \to \infty$, the clusters shrink to two separated points (Fig. 1D). Here, the temperature approaches the limiting supercondensate temperature T_s, which is independent of geometry (*17*), and the dipole moment approaches a maximum D_s, determined by the geometry. In a superfluid, the cutoff scale ξ is provided by the superfluid healing length; vortex-core repulsion at lengths ~ξ prevents the eventual point collapse at infinite energy by enforcing an upper energy limit with a minimum entropy (*14*).

To physically realize this idealized model, the vortices must form a well-isolated subsystem and effectively decouple from the other fluid degrees of freedom. A large and uniform 2D Bose-Einstein condensate (BEC), near zero temperature with weak vortex-sound coupling, has been proposed as a suitable candidate system (*18*–*21*). Furthermore, superfluids allow for vortex-antivortex annihilation, which favors the formation of Onsager vortices through evaporative heating (*20*, *22*), whereby annihilations remove low-energy dipoles, thus increasing the remaining energy per vortex. However, although small transient clusters have been observed in BEC (*23*–*25*), attempts to create Onsager's vortex clusters have thus far been hindered by thermal dissipation and vortex losses at boundaries (*26*), which are enhanced by fluid inhomogeneities (*27*). This has prevented the experimental study of the full phase diagram of 2D vortex matter shown in Fig. 1.

We overcome these issues by working with a uniform planar ^{87}Rb BEC confined to an elliptical geometry (*14*). Although the BEC itself is three-dimensional, the vortex dynamics are two-dimensional owing to the large energy cost of vortex bending (*14*, *28*). By engineering different stirring potentials, we can efficiently inject vortex configurations with minimal sound excitation (*14*). A high-energy vortex configuration can be injected using a double-paddle stir, whereby two narrow potential barriers (*29*, *30*) are swept along the edges of the trap (Fig. 2A). Because of the broken symmetry of the ellipse, the maximum entropy state is a vortex dipole separated along the major axis (*31*). The stirring protocol is well mode-matched to this vorticity distribution, and we find that the vortices rapidly organize into two Onsager vortex clusters (Fig. 2B).

We contrast these results with the injection of a low-energy configuration from sweeping

[1]Australian Research Council Centre of Excellence for Engineered Quantum Systems, School of Mathematics and Physics, University of Queensland, St. Lucia, QLD 4072, Australia. [2]Australian Research Council Centre of Excellence in Future Low-Energy Electronics Technologies, School of Mathematics and Physics, University of Queensland, St. Lucia, QLD 4072, Australia. [3]Department of Physics, Centre for Quantum Science, and Dodd-Walls Centre for Photonic and Quantum Technologies, University of Otago, Dunedin 9016, New Zealand.
*These authors contributed equally to this work.
†Corresponding author. Email: t.neely@uq.edu.au

Downloaded from http://science.sciencemag.org/ on April 23, 2021

a grid of smaller circular barriers through the BEC. Experimentally, we find that this results in a similar number of vortices (Fig. 2, D and E), but in a disordered distribution that can undergo evaporative heating (*20*, *27*, *32*) (Fig. 1B). Gross-Pitaevskii equation (GPE) simulations quantitatively model both stirring methods and are compared in Fig. 2, C and F, and movies S1 and S2.

Although the detection of the vortex sign (*26*, *32*) is possible (*14*), the clustered states are nonuniform equilibria, and their presence can also be confirmed from the (unsigned) vortex density $\rho = \sigma_+ + \sigma_-$, where σ_+ (σ_-) denotes the distribution of positive (negative) vortices (*14*). Figure 3A displays a time-averaged position histogram, generated by measuring the experimental vortex positions at 1-s intervals over 10 s of hold time after injection. As expected for our elliptical geometry (*14*), the density shows two distinct persistent clusters separated along the major axis. The clusters remain distinguishable up to 9 s of hold time in individual frames (see movie S3). By contrast, the grid stir in Fig. 3B shows a near-uniform distribution of vortices consistent with an unclustered phase (Fig. 1, A and B). Figure 3, C and D, shows the corresponding (signed) density $\omega = \sigma_+ - \sigma_-$ from GPE simulations, showing polarized clusters for the paddle stir, contrasted with $\omega \approx 0$ for the grid stir. Figure 3E shows the total vortex number as a function of time for the two stirs in comparison with respective simulations. The vortex number for the paddle stir shows almost complete suppression of vortex decay over 10 s, indicating a strong spatial segregation of oppositely signed vortices. In contrast, the grid stir loses 60% of the vortices over this period to vortex annihilation and edge losses. Figure 3F plots the vortex nearest-neighbor distance ℓ/ℓ_0 (where $\ell/\ell_0 \simeq 1$ indicates a uniform distribution) (Fig. 1E). Although this quantity increases with time for the clustered state, indicating spreading of the clusters, it remains <1 for the entire 10-s duration. By contrast, for the grid stir, ℓ/ℓ_0 stays quasi-constant and near unity, which is characteristic of a disordered state.

In the clustered phase, our simulations demonstrate that vortex signs can be dependably inferred for $t \leq 5$ s from the experimental positions of the vortices relative to the minor axis of the ellipse (*14*). From these data we can estimate the energy of the experimental vortex configurations as a function of time using the point-vortex model [including boundary effects (*14*)] and compare with GPE simulations, as shown in Fig. 3G. Despite a gradual decay of the energy, the system remains well within the negative temperature clustered region for the entire 10-s hold time, equivalent to ~50 times the initial cluster turnover time of ~0.2 s (see movie S1). The decay is caused by a combination of the finite lifetime of the condensate ($\tau = 28 \pm 2$ s), residual thermal fraction of ~30%, and residual nonuniform BEC density of ~6% root mean square. This conclusion is supported by GPE simulations with phenomenological damping, which are in agreement with experimental observations (see Fig. 3G). The grid-stir simulation shows a small increase

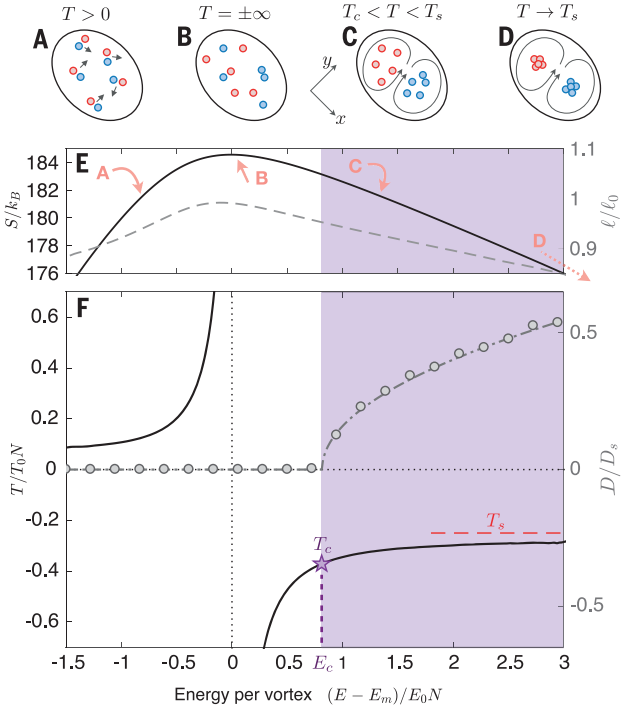

Fig. 1. Phases of point-vortex matter in a bounded domain. (**A**) Small positive temperatures exhibit bound vortex-antivortex pairs. (**B**) As the vortex temperature $T \to \infty$, vortex positions become uncorrelated. (**C**) At sufficiently high energies, a clustering temperature T_c is reached where giant Onsager vortex clusters form. (**D**) As $E \to \infty$, the clusters shrink to two separated points, forming a supercondensate. (**E** and **F**) Monte Carlo data for a neutral vortex gas, for the elliptical domain and vortex numbers ($N_+ = N_- = N/2 = 9$) studied in the experiment. (E) Entropy S and nearest-neighbor distance ℓ/ℓ_0, where $\ell_0 = \sqrt{ab/N}$ for ellipse semi-major axis a and semiminor axis b. (F) Temperature T and the dipole moment (order parameter of the clustering transition) $D = N^{-1}\left|\sum_j \mathrm{sgn}(\Gamma_j)x_j\right|$ as a fraction of the supercondensate limit $D_s \approx 0.47a$ (*14*). Above the transition, $D \propto (E - E_c)^{1/2}$ (*14*) and a line of best fit yields the transition point $(E_c - E_m) \approx 0.81E_0N$, $T_c \approx -0.37T_0N$ (purple star); the shaded region exhibits macroscopic vortex clusters. The red dashed line indicates the supercondensation limit, $E \to \infty$, $T \to T_s = -0.25T_0N$. Here, $E_0 = \rho_0\Gamma^2/4\pi$ and $T_0 = E_0/k_B$.

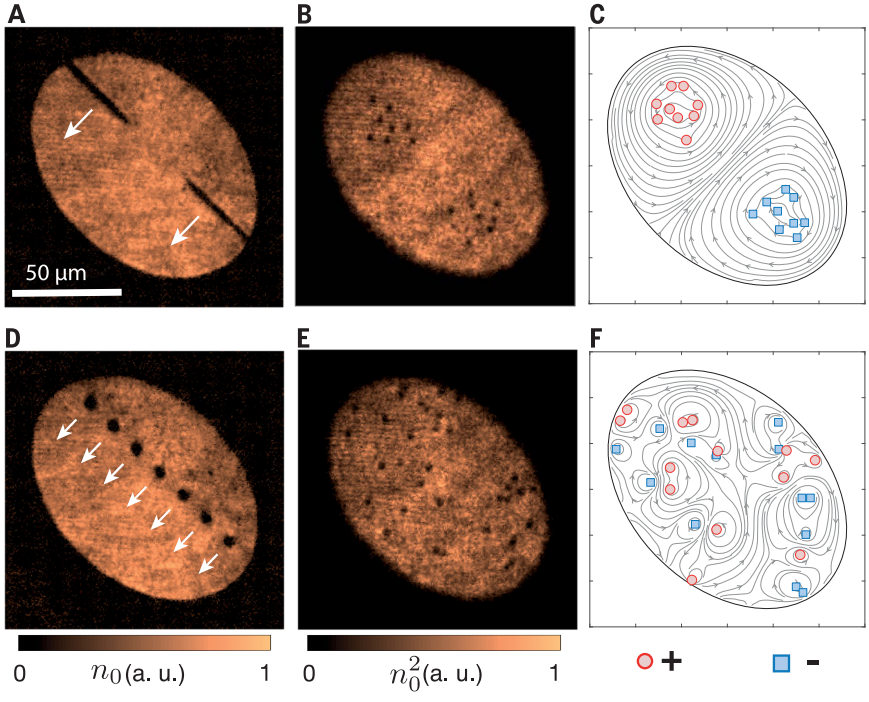

Fig. 2. Experimental vortex injection. (**A**) Two large paddle potentials stir the BEC inducing large-scale flow (in situ image, partway through the stir). The white arrows indicate the direction of the stir. (**B**) A 3-ms time-of-flight Faraday image directly after the paddle stir clearly resolves injected vortices (*14*) localized into two clusters. (**C**) Simulation of the paddle stir showing velocity contours, with the location and circulations of the vortices demonstrating the injection of a clustered vortex dipole. (**D** to **F**) As for (A to C), but with a low-energy vortex distribution injected by a grid of narrow circular barriers. a.u., arbitrary units.

Downloaded from http://science.sciencemag.org/ on April 23, 2021

in energy per vortex over the hold time, indicating that evaporative heating marginally prevails over thermal dissipation; annihilations manage to drive the system toward the negative temperature region but not into the clustered phase.

Similarly, we estimate the dipole moment D and the vortex temperature T, which we compare with theoretical predictions. Figure 3H shows that the paddle stir exhibits a large dipole moment, with an average of $D/D_s \sim 81\%$ over the 10-s hold time. The experimental estimate agrees well with simulations for $t \leq 5$ s, when opposite-signed vortices remain completely segregated on opposite sides of the minor axis. By contrast, for the grid stir, $D/D_s \sim 1/\sqrt{N}$, which is consistent with an unclustered phase at finite N (*14*, *16*). Finally, our Monte Carlo simulations (*14*) show that the clustering transition occurs at a temperature $T_c \simeq -0.37T_0N$, whereas supercondensation (*16*) occurs at $T_s = -0.25T_0N$ (see Fig. 1F). We estimate the final temperature from the point-vortex energy as $T_{exp} \simeq -0.28T_0N$, which is consistent with the vortex system being in the clustered region of the phase diagram.

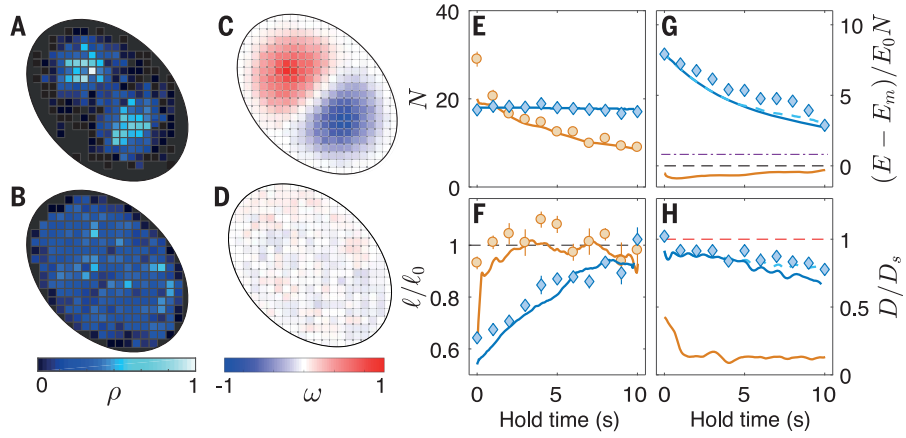

Fig. 3. Evidence of vortex cluster metastability. Experimental (unsigned) vortex density histograms $\rho = \sigma_+ + \sigma_-$ for (**A**) paddle and (**B**) grid stirs, respectively. The data are collected after hold times of $t = \{0, 1, 2, \ldots 10\}$ seconds, with 10 samples at each time point (110 samples total). (**C** and **D**) Corresponding GPE simulation (signed) vorticity histograms $\omega = \sigma_+ - \sigma_-$ time averaged over 0 to 10 s. (**E** and **F**) Experimental average vortex number $\langle N \rangle$ and nearest-neighbor distance ℓ/ℓ_0 versus hold time, where $\ell_0 = \sqrt{0.89ab/N}$ is the expected value for a uniform distribution within the 89% detection region of the a:b ratio ellipse: paddle stir (blue diamonds) and grid stir (orange circles). GPE simulation results are shown as solid lines of the same color. (**G**) Point-vortex energy versus time. Blue diamonds: experimental estimate. Blue solid line: exact point-vortex energy from GPE. Blue dashed line: estimate from applying the experimental vortex classification method to the GPE data. The black dashed line indicates the energy of the state with $T = \pm\infty$ and the purple dash-dotted line indicates $T = T_c$. The orange line indicates the energy of the grid-stir simulation. (**H**) Dipole moment versus time. Lines and markers are as in (G). Red dashed line shows the supercondensate limit $D = D_s$. Simulations are averaged over 10 runs and a 1-s rolling time average.

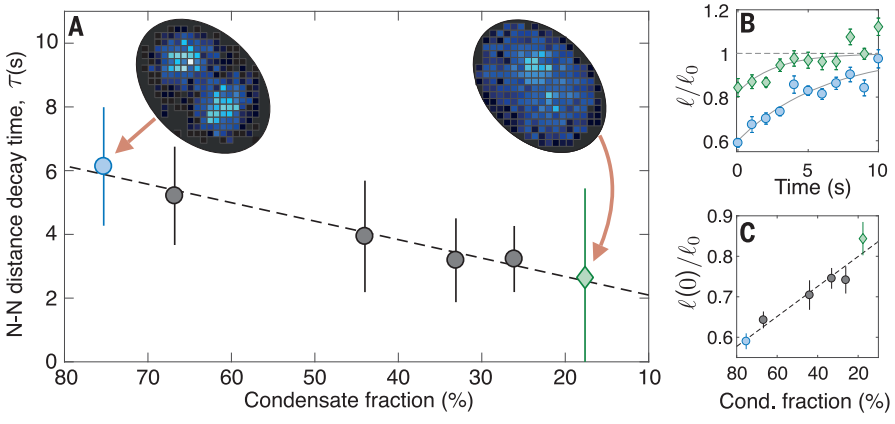

Fig. 4. Cluster decay rate versus BEC fraction. (**A**) Decreasing condensate fraction results in more-rapid cluster dissociation, indicated by decreasing nearest-neighbor (N-N) distance decay times, as determined by exponential fits. (**B**) N-N distance decay for the largest (blue circles) and smallest (green diamonds) condensate fractions, with fits shown by solid lines. Insets in (A) show time-averaged vortex density histograms accumulated over a 10-s hold for these cases, as in Fig. 3; see fig. S7 for the full set of time-averaged histograms and fig. S8 for the histograms immediately following the stir. (**C**) The initial N-N distance $\ell(0)$ increases with decreasing condensate fraction, indicating limitations in injecting high-vortex energy in the presence of thermal damping. The dashed line indicates a linear fit to the data.

Thermal friction is expected to play a major role in the damping of the Onsager vortex clusters (*33*). We experimentally investigated the role of an increased thermal component by injecting clusters for a range of smaller condensate fractions (i.e., higher BEC temperatures) while maintaining a similar injected vortex number (fig. S9). As shown in Fig. 4A, with decreasing condensate fraction we observe a reduction of the exponential decay time nearest-neighbor distance decay time to the uniform value $\ell/\ell_0 \simeq 1$, obtained by empirical fits to the nearest-neighbor distance (*14*) (examples in Fig. 4B). These results indicate that, with decreasing condensate fraction, the vortices more rapidly approach a low-energy, uncorrelated distribution; cumulative vortex histograms for the largest and smallest condensate fractions (Fig. 4A, insets) also show diminished clustering with decreasing condensate fraction. Furthermore, the initial nearest-neighbor distance increases with decreasing condensate fraction (Fig. 4C), suggesting that the injection of high-energy clusters is less efficient with increased damping. These results suggest thermal dissipation is more important than losses to sound in our experiment; indeed, Gross-Pitaevski simulations without thermal damping (thus containing only losses from vortex-sound coupling) were found to support this conclusion as the clusters retained >90% of their initial energy (*14*). Thermal friction may limit the observation of dynamic emergence of Onsager vortex clusters in future experiments.

Once achieved, the clustered phase is remarkably robust to dissipation, contrary to the conventional wisdom for negative temperature states. Meanwhile, the evaporative heating mechanism appears to be more fragile, inhibited by modest dissipation. Nonetheless, a systematic study of the clustering transition and its emergence from quantum turbulence (*19*–*21*) appears within reach if further reduction of thermal dissipation can be achieved. The precise control of the trapping potential in our experiment enables a broad range of stirring and trapping configurations, opening the door to additional studies of the vortex-clustering phase transition (*16*, *19*, *20*) and of fully developed quantum turbulence confined to two dimensions. Emerging tools for precision characterization, including vortex circulation detection (*26*), momentum spectroscopy (*34*), and correlation functions (*29*, *35*), can be expected to provide further insights into the role of coherent structures in 2D vortex matter.

Downloaded from http://science.sciencemag.org/ on April 23, 2021

We note that negative absolute temperature vortex states in a different regime, along with signatures of evaporative heating by vortex-antivortex annihilation, were independently observed in (*32*).

REFERENCES AND NOTES

1. R. H. Kraichnan, D. Montgomery, *Rep. Prog. Phys.* **43**, 547–619 (1980).
2. D. Montgomery, G. Joyce, *Phys. Fluids* **17**, 1139 (1974).
3. R. H. Kraichnan, *Phys. Fluids* **10**, 1417 (1967).
4. L. Onsager, *Nuovo Cim.* **6** (S2), 279–287 (1949).
5. C. C. Lin, *Proc. Natl. Acad. Sci. U.S.A.* **27**, 570–575 (1941).
6. J. Maurer, P. Tabeling, *Europhys. Lett.* **43**, 29–34 (1998).
7. E. A. Henn, J. A. Seman, G. Roati, K. M. F. Magalhães, V. S. Bagnato, *Phys. Rev. Lett.* **103**, 045301 (2009).
8. M. A. Rutgers, *Phys. Rev. Lett.* **81**, 2244–2247 (1998).
9. R. A. Smith, T. M. O'Neil, *Phys. Fluids B* **2**, 2961–2975 (1990).
10. J. Binney, S. Tremaine, *Galactic Dynamics* (Princeton Univ. Press, 2011).
11. R. M. Young, P. L. Read, *Nat. Phys.* **13**, 1135–1140 (2017).
12. P. Tabeling, *Phys. Rep.* **362**, 1–62 (2002).
13. J. Sommeria, in *New Trends in Turbulence*, M. Lesieur, A. M. Yaglom, F. David, Eds. (Springer, 2001), pp. 385–447.
14. See supplementary materials for details.
15. Adding a finite vortex-core size allows the Kosterlitz-Thouless transition to occur in this system (*36*).
16. X. Yu, T. P. Billam, J. Nian, M. T. Reeves, A. S. Bradley, *Phys. Rev. A* **94**, 023602 (2016).
17. R. H. Kraichnan, *J. Fluid Mech.* **67**, 155–175 (1975).
18. A. L. Fetter, *Phys. Rev.* **151**, 100–104 (1966).
19. T. P. Billam, M. T. Reeves, B. P. Anderson, A. S. Bradley, *Phys. Rev. Lett.* **112**, 145301 (2014).
20. T. Simula, M. J. Davis, K. Helmerson, *Phys. Rev. Lett.* **113**, 165302 (2014).
21. H. Salman, D. Maestrini, *Phys. Rev. A* **94**, 043642 (2016).
22. L. Campbell, K. O'Neil, *J. Stat. Phys.* **65**, 495–529 (1991).
23. T. W. Neely, E. C. Samson, A. S. Bradley, M. J. Davis, B. P. Anderson, *Phys. Rev. Lett.* **104**, 160401 (2010).
24. T. W. Neely *et al*., *Phys. Rev. Lett.* **111**, 235301 (2013).
25. W. J. Kwon, J. H. Kim, S. W. Seo, Y. Shin, *Phys. Rev. Lett.* **117**, 245301 (2016).
26. S. W. Seo, B. Ko, J. H. Kim, Y. Shin, *Sci. Rep.* **7**, 4587 (2017).
27. A. J. Groszek, T. P. Simula, D. M. Paganin, K. Helmerson, *Phys. Rev. A* **93**, 043614 (2016).
28. S. J. Rooney, P. B. Blakie, B. P. Anderson, A. S. Bradley, *Phys. Rev. A* **84**, 023637 (2011).
29. A. C. White, C. F. Barenghi, N. P. Proukakis, *Phys. Rev. A* **86**, 013635 (2012).
30. G. W. Stagg, N. G. Parker, C. F. Barenghi, *J. Phys. B At. Mol. Opt. Phys.* **47**, 095304 (2014).
31. J. G. Esler, T. L. Ashbee, *J. Fluid Mech.* **779**, 275–308 (2015).
32. S. P. Johnstone *et al*., *Science* **364**, 1267–1271 (2019).
33. G. Moon, W. J. Kwon, H. Lee, Y.-i. Shin, *Phys. Rev. A* **92**, 051601 (2015).
34. M. T. Reeves, T. P. Billam, B. P. Anderson, A. S. Bradley, *Phys. Rev. A* **89**, 053631 (2014).
35. A. Skaugen, L. Angheluta, *Phys. Rev. E* **93**, 042137 (2016).
36. J. M. Kosterlitz, D. J. Thouless, *J. Phys. C Solid State Phys.* **6**, 1181–1203 (1973).
37. G. Gauthier *et al*., Giant vortex clusters in a two-dimensional quantum fluid: Data sets, Version 1.0, Zenodo (2019); http://doi.org/10.5281/zenodo.2548958.
38. UQBEC, UQBEC/GiantVortices: Giant vortex clusters in a two-dimensional quantum fluid, Version 1.0, Zenodo (2019); http://doi.org/10.5281/zenodo.2667866.

ACKNOWLEDGMENTS

We thank B. P. Anderson, L. A. Williamson, P. B. Blakie, K. Helmerson, T. Simula, S. P. Johnstone, A. J. Groszek, M. Cawte, and G. J. Milburn for useful discussions. **Funding:** This research was partially supported by the Australian Research Council through the ARC Centre of Excellence for Engineered Quantum Systems (project numbers CE1101013 and CE170100009), the ARC Centre of Excellence in Future Low-Energy Electronics Technologies (project number CE170100039), and ARC Discovery Project DP160102085 and was also funded by the Australian Government. Further support was provided by the Dodd-Walls Centre for Photonic and Quantum Technologies, the Royal Society of New Zealand Marsden Fund (contract UOO1726). T.A.B. and G.G. acknowledge the support of an Australian Government Research and Training Program Scholarship. **Author contributions:** G.G. and T.W.N. conducted the experiments. M.T.R., A.S.B., X.Y., M.J.D., and T.W.N. conceived of the experiment and wrote the manuscript. Simulations were run by M.T.R., G.G., and T.A.B. Analysis of the experimental data within the analytical theory was carried out by X.Y., M.T.R., and A.S.B. The experimental apparatus was built by T.W.N., G.G., M.A.B., and H.R.-D. All authors commented on the experiments and the manuscript. **Competing interests:** The authors declare no competing interests. **Data and materials availability:** All data shown in this work and simulation scripts can be found at Zenodo (*37*, *38*).

SUPPLEMENTARY MATERIALS

science.sciencemag.org/content/364/6447/1264/suppl/DC1
Materials and Methods
Figs. S1 to S9
References (*39*–*50*)
Movies S1 to S3

14 March 2018; accepted 6 June 2019
10.1126/science.aat5718

Downloaded from http://science.sciencemag.org/ on April 23, 2021

Science

Giant vortex clusters in a two-dimensional quantum fluid

Guillaume Gauthier, Matthew T. Reeves, Xiaoquan Yu, Ashton S. Bradley, Mark A. Baker, Thomas A. Bell, Halina Rubinsztein-Dunlop, Matthew J. Davis and Tyler W. Neely

Science **364** (6447), 1264-1267.
DOI: 10.1126/science.aat5718

Clustering vortices

Many-body systems generally become more disordered as more energy is pumped into them. A curious exception to this rule was predicted in the context of turbulent flow by the physical chemist Lars Onsager. He suggested that the entropy of certain two-dimensional (2D) systems can decrease with increasing energy, corresponding to an effective negative temperature. Using 2D Bose-Einstein condensates of atoms, Gauthier *et al.* and Johnstone *et al.* put Onsager's theory to the test. They provided energy to the system by perturbing the condensate, creating vortices and antivortices. With increasing energy, the system became more ordered as clusters containing either only vortices or only antivortices emerged.

Science, this issue p. 1264, p. 1267

ARTICLE TOOLS http://science.sciencemag.org/content/364/6447/1264

SUPPLEMENTARY MATERIALS http://science.sciencemag.org/content/suppl/2019/06/26/364.6447.1264.DC1

REFERENCES This article cites 46 articles, 2 of which you can access for free
http://science.sciencemag.org/content/364/6447/1264#BIBL

PERMISSIONS http://www.sciencemag.org/help/reprints-and-permissions

Use of this article is subject to the Terms of Service

Science (print ISSN 0036-8075; online ISSN 1095-9203) is published by the American Association for the Advancement of Science, 1200 New York Avenue NW, Washington, DC 20005. The title *Science* is a registered trademark of AAAS.

Copyright © 2019 The Authors, some rights reserved; exclusive licensee American Association for the Advancement of Science. No claim to original U.S. Government Works

Downloaded from http://science.sciencemag.org/ on April 23, 2021